Influence of the seabed conditions on the near-and far-field propagation of noise in impact piling

Tsouvalas, Apostolos; Peng, Yaxi; Metrikine, Andrei V.

Publication date
2021

Document Version
Accepted author manuscript

Published in
"Advances in Acoustics, Noise and Vibration - 2021"

Citation (APA)
Tsouvalas, A., Peng, Y., & Metrikine, A. V. (2021). Influence of the seabed conditions on the near-and far-field propagation of noise in impact piling. In E. Carletti, M. Crocker, M. Pawelczyk, & J. Tuma (Eds.), *"Advances in Acoustics, Noise and Vibration - 2021" : Proceedings of the 27th International Congress on Sound and Vibration, ICSV 2021* Article 90 Silesian University Press.
https://iiav.org/content/archives_icsv_last/2021_icsv27/content/papers/papers/full_paper_90_20210413104141430.pdf

Important note
To cite this publication, please use the final published version (if applicable).
Please check the document version above.

27th International Congress
on Sound and Vibration
The annual congress of
the International Institute
of Acoustics and Vibration (IIAV)

11-16 July, 2021

ICSV27

Annual Congress of the International Institute of Acoustics and Vibration (IIAV)

INFLUENCE OF THE SEABED CONDITIONS ON THE NEAR- AND FAR-FIELD PROPAGATION OF NOISE IN IMPACT PILING

Apostolos Tsouvalas, Yaxi Peng, Andrei V. Metrikine
Faculty of Civil Engineering and Geosciences, Delft University of Technology, Stevinweg 1, 2628 CN Delft, The Netherlands
e-mail: A.Tsouvalas@tudelft.nl

The prediction of underwater noise and the assessment of the influencing factors on noise transmission are significant for the control and mitigation of the noise generated by offshore pile driving. This paper presents a coupled two-step approach for modelling the underwater noise from offshore pile driving, with the focus being placed on examining the influence of the seabed conditions on the near- and far-field sound propagation. The complete model consists of a near-source module and a far from source module. The near-source module captures the coupled vibroacoustic behaviour of the pile and its surrounding fluid and layered soil media. With the input obtained from near-source module, the far-from-source module propagates the sound field at larger distances. The two modules are coupled by applying the boundary integral method. A parametric study is performed to investigate the influence of the seabed properties on the noise levels and the energy distribution at various horizontal distances from the pile. An energy flux analysis is performed by examining the total energy radiated through the cylindrical surface at target distances from the pile. As waves propagate away from the pile, the through-depth distribution of the energy in both seawater and sediment alters. The results indicate the characteristics of noise transmission and energy distribution with respect to different soil conditions; an analysis which is key to the development of effective noise mitigation strategies.
Keywords: underwater noise, offshore pile driving, seabed conditions, vibro-acoustics, noise propagation

1. Introduction

The underwater noise generated during the installation of foundation piles offshore has been an issue of serious concern mainly due to the rapid developments in the offshore wind industry. The noise pollution itself poses a threat to the marine fauna [1]. In order to comply with the strict regulations imposed by several countries, the offshore industry strives to keep the noise levels to within acceptable limits. To assist the control of hydro-sound emission, underwater noise prediction becomes essential in order to assess the noise levels to be expected during the installation of new foundation piles.

Over the past decade, several models have been developed for noise prediction due to impact piling [2]. Reinhall and Dahl [3] were the first to examine systematically the noise generated by impact piling by using a Finite Element (FE) model for the noise generation in the vicinity of the pile and a Parabolic Equation (PE) model for the noise propagation at larger distances. In most available models to date [2], a two-step approach similar to [3] is adopted to model the entire noise path from the noise source to the receiver. In contrast to the aforementioned models, a semi-analytical approach for the prediction of underwater noise from pile driving was developed by Tsouvalas and Metrikine [4] based on a mode-matching

algorithm. The latter includes, additionally, a three-dimensional description of the seabed allowing one to investigate the influence of the seabed properties on the noise generation and transmission.

In this paper, the authors examine the influence of the seabed conditions on the near and far-field propagation of noise in impact piling. A computationally efficient method is presented for the prediction of the generation and propagation of the sound field associated with impact piling at large distances [5, 6]. The method extends the earlier works [7] by a far-range propagation module [6]. The complete model consists of two modules: i) a near-source module aiming at the accurate description of the pile-water-soil interaction together with the sound generation and propagation in the pile vicinity [4]; and ii) a far-from-source module aiming at the propagation of the wave field at larger distances[6]. The input to the far-from-source module is provided by the near-source module through a boundary integral formulation. An energy flux analysis is performed to examine the total energy radiated into the water and the seabed at various distances from the pile.

Section 2 introduces the mathematical statement of the problem together with the underlying assumptions while in section 3, the solution technique is presented. In section 4, a parametric case study is conducted focusing on the influence of the seabed properties on the noise generation and propagation. Finally, section 5 gives an overview of the main conclusions of the paper.

2. Description of the model and governing equations

The complete model is shown in Fig. 1. The near-source module consists of the pile, which is modelled as linear elastic thin shell, and the surrounding media modelled as a horizontally stratified acousto-elastic waveguide. The hammer and anvil are not modelled; instead, they substituted by a forcing function $F(t)$ applied at the pile head. The shell is of finite length and occupies the domain $0 \leq z \leq L$. The fluid is modelled as a three-dimensional inviscid compressible medium with a compressional wave speed c_f and a density ρ_f occupying the region $z_0 \leq z \leq z_1$ and $r \geq R$. The soil is described as a three-dimensional horizontally stratified elastic continuum. Each soil layer is characterised by its density ρ_j and the compressional and shear wave speeds $c_{p,j}$ and $c_{s,j}$, respectively. In the near-source module, the soil occupies the domain $z \geq z_1$ and is terminated at a large depth $z = H$ with a rigid boundary which has been shown not to affect the pile vibrations (and thus the noise generation mechanism) significantly [4]. In the far-from-source module, the soil extends to infinity in the vertical direction as well to accurately capture the energy loss mechanisms at larger distances from the pile.

The equations of motion of the pile-soil-water system are given as [7]:

$$\mathbf{L}\,\mathbf{u}_p + \mathbf{I}_m\,\ddot{\mathbf{u}}_p = -\left[H(z-z_0) - H(z-L)\right]\,\mathbf{t}_s + \mathbf{f} \tag{1}$$

$$G_j\,\nabla^2\mathbf{u}_s^j + (\lambda_j + G_j)\,\nabla\nabla\cdot\mathbf{u}_s^j - \rho_j\ddot{\mathbf{u}}_s^j = \mathbf{0} \tag{2}$$

$$\nabla^2\phi_f(r,z,t) - \frac{1}{c_f^2}\ddot{\phi}_f(r,z,t) = 0 \tag{3}$$

In the equations above, $\mathbf{u}_p = \left[u_{p,z}(z,t)\ u_{p,r}(z,t)\right]^{\mathrm{T}}$ is the displacement vector of the mid-surface of the shell, $\mathbf{u}_s^j(r,z,t) = \left[u_{s,z}^j(r,z,t)\ u_{s,r}^j(r,z,t)\right]^{\mathrm{T}}$ is the displacement vector of each solid layer and $\phi_f(r,z,t)$ is a velocity potential introduced for the description of the fluid. The operators $\mathbf{L}$ and $\mathbf{I}_m$ are the stiffness and modified inertia matrices, respectively [4]. The vector $\mathbf{t}_s$ represents the boundary stress vector that takes into account the reaction of the soil and fluid surrounding the shell at $z_0 < z < L$. Naturally, for the domain $z_0 < z < z_1$ this reflects only the normal pressure exerted by the fluid normal to the surface whereas for the region $z > z_1$ both shear and normal stresses are present. The functions $H(z - z_i)$ are the Heaviside step functions which are used here to account for the fact that the soil and the fluid are in

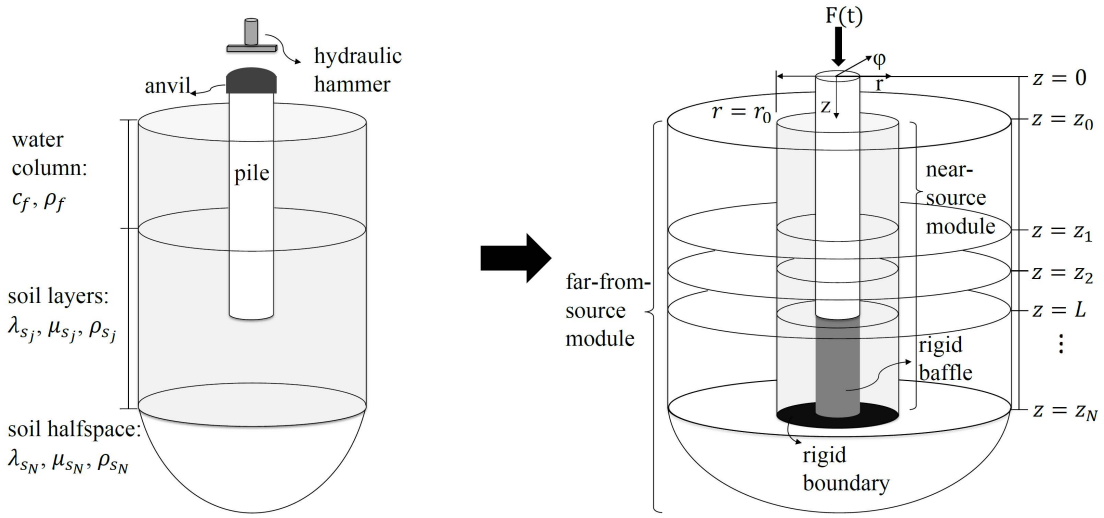

Figure 1: Geometry of the complete system (left) and the coupled modelling approach (right).

contact with a segment of the shell in correspondence with Fig. 1. The vector $\mathbf{f} = [f_{rz}(z,t)\ f_{rr}(z,t)]^{\mathrm{T}}$ represents the externally applied force on the surface of the shell.

The various solid layers are in full contact with each other at the horizontal interfaces. At the soil-water interface, the vertical stress equilibrium and the vertical displacement continuity are imposed, whereas the shear stress at the surface of the upper solid layer vanishes. A set of boundary conditions and interface conditions are formulated as follows for $r \geq R$:

$$p_f(r, z_0, t) = 0 \tag{4}$$

$$\sigma^1_{s,zz}(r, z_1, t) + p_f(r, z_1, t) = 0,\ \sigma^1_{s,zr}(r, z_1, t) = 0,\ u^1_{s,z}(r, z_1, t) - v_{f,z}(r, z_1, t) = 0 \tag{5}$$

$$\sigma^{j+1}_{s,zi}(r, z_j, t) - \sigma^j_{s,zi}(r, z_j, t) = 0,\ u^{j+1}_{s,i}(r, z_j, t) - u^j_{s,i}(r, z_j, t) = 0\,,\ 2 \leq j \leq N-1,\ i = z, r \tag{6}$$

$$u^N_{s,r}(r, z_N, t) = u^N_{s,z}(r, z_N, t) = 0 \tag{7}$$

The terms $\sigma^j_{s,zi}(r, z, t)$ represent the stresses in the soil at the corresponent layer j. In addition to Eqs. (4–7) above, the radiation condition needs to be satisfied at $r \to \infty$. In the far-from-source module, the boundary conditions at $z = z_N$ are substituted by the radiation condition at $z \to \infty$ (lower soil layer is a half space).

3. Solution approach

The solution approach consists of two steps. First, the solution to the vibro-acoustic problem in the near-source module is considered to obtain the response of the system in the pile vicinity. Since this step has been described in earlier works [4, 7], the solution technique is only briefly covered here. Second, the Green's tensor is derived for sources positioned in the fluid and in the seabed and a method is presented which allows the coupling of the two modules.

3.1 Near-source module

The semi-analytical model developed by Tsouvalas and Metrikine [4] forms the basis of the near-source module. Since the coupled vibroacoustic system is linear, a solution in the frequency domain

suffices. Both shell and acousto-elastic responses are expressed in terms of modes satisfying the conditions along the z-coordinate:

$$\tilde{u}_{p,k}(z,\omega) = \sum_{m=1}^{\infty} A_m \, U_{km}(z) \,, \tag{8}$$

in which $k = r; z$ refers to the different displacement components while $m = 1, 2, ..., \infty$ is an index defining the mode number. The vertical eigenfunctions $U_{km}(z)$ satisfy the boundary conditions at $z = 0$ and $z = L$. The expression for the pressure in the seawater, which inherently satisfies the boundary and interface conditions along the vertical coordinate, as well as the radiation condition at $r \to \infty$ reads:

$$\tilde{p}(r,z,\omega) = \sum_{p=1}^{\infty} C_p \, H_0^{(2)}(k_p r) \, \tilde{p}_{f,p}(z) \,, \tag{9}$$

in which $H_0^{(2)}$ denotes the 0^{th}-order Hankel function of the second kind which ensures that the radiation condition at $r \to \infty$ is satisfied at all times. The coefficients C_p with $p = 1, 2, ..., \infty$ are the unknown modal amplitudes while $\tilde{p}_{f,p}(z)$ define the known (by means of solution of the eigenvalue problem posed [8]) pressure eigenfunctions. The displacement and stress fields in the seabed can be expressed in similar manner; these expressions are omitted here for the sake of brevity. The terms k_p denote the horizontal wavenumber obtained by the formulation of the eigenvalue problem as discussed in [4]. In Eqs. (8–9), the only unknowns are the coefficients of the modal expansions A_m and C_p. A system of infinite algebraic equations with respect to the unknown coefficients C_p can be obtained as explained in [7]:

$$\sum_{q=1}^{\infty} C_q \left(L_{qp} + k_q \, H_1^{(2)}(k_q R) \, \Gamma_q \, \delta_{qp} - \sum_{m=1}^{\infty} \frac{R_{mq} \, Q_{mp}}{I_m} \right) = \sum_{m=1}^{\infty} \frac{F_m \, Q_{mp}}{I_m} \tag{10}$$

The coefficients of the shell structure are given by:

$$A_m = \frac{F_m + \sum_{p=1}^{\infty} C_p \, R_{mp}}{I_m} \tag{11}$$

A detailed derivation of the terms L_{qp}, Γ_q, Q_{mp}, R_{mp} and I_m introduced in Eqs. (10) and (11) is given in [4]. Due to the fact that the eigensolutions of the shell and acousto-elastic waveguide need to be solved only once for a certain configuration of soil layers, the examination of various installation scenarios is computationally very fast. By coupling the near-source module to the far-from-source module, the complete model can also treat accurately complex soil conditions over larger radial distances as will be seen in the sequel.

3.2 Far-from-source module

The basis of the far-from-source model is the built-up of the Green's matrix for the acousto-elastic system in which the excitation is a ring source positioned at a given radius and depth (either in the soil or in the fluid). Let us assume that a ring source is positioned at r_0, z_0 as shown in Fig. 2(a). Without loss of generality, the procedure is described in detail for the derivation of one of the components of the Green's matrix. The equations of motion of the acousto-elastic domain (in the frequency domain) are given as:

$$[\nabla^2 + k_\xi^2]\tilde{G}(r,z;r_0,z_0,\omega) = S_\beta^\xi(\omega)\frac{\delta(r-r_0, z-z_0)}{2\pi r} \tag{12}$$

The delta function $\delta(r - r_0, z - z_0)$ represents the source term [9] while k_ξ with index $\xi = f, p_j$ or s_j represent the medium wavenumbers, i.e. $k_f = \omega/c_f, k_{p,j} = \omega/c_{p,j}, k_{s,j} = \omega/c_{s,j}$. $S^\xi_\beta(\omega)$ represents the source strength, which is determined such that a unit impulse is applied along the β-direction ($\beta = z; r$).

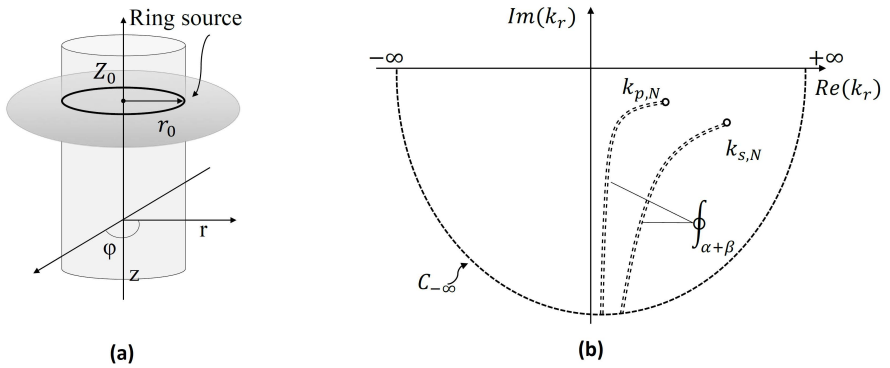

Figure 2: (a) Representation of the ring source; (b) complex wavenumber plane and EJP branch cuts.

Application of the forward Hankel transform to Eq. (12) yields:

$$\left[\frac{d^2}{dz^2} + k^2_{z,\xi}\right] \hat{G}(k_r, z; r_0, z_0, \omega) = S^\xi_\beta(\omega) \frac{J_0(k_r\, r_0)}{2\pi}\, \delta(z - z_0) \tag{13}$$

in which: $k_{z,\xi} = \sqrt{k^2_\xi - k^2_r}$. $\tilde{G}$ and $\hat{G}$ denote the Green's functions in frequency and Hankel domains, respectively. Once the solution in the Hankel domain is known, the inverse Hankel transform yields:

$$\tilde{G}(r, z; r_0, z_0, \omega) = -\frac{1}{2}\int_{-\infty}^{+\infty} \left(S^\xi_\beta(\omega) \frac{e^{-\mathrm{i}k_{z,\xi}|z-z_0|}}{4\pi \mathrm{i} k_(z,\xi)} + A^1_\xi e^{\mathrm{i}k_{z,\xi}z} + A^2_\xi e^{-\mathrm{i}k_{z,\xi}z} \right) J_0(k_r\, r_0) H^{(2)}_0(k_r\, r) k_r dk_r \tag{14}$$

For $z \geq z_N$, $A^1_\xi = 0$ to ensure that the out-going waves *leave* the soil half-space without reflection. Upon substitution of the above solutions into the boundary and interface conditions given by Eqs. (4–6), it is straightforward that the kernels in the integral representations need to be satisfied. This yields a linear algebraic system with unknowns A^1_ξ and A^2_ξ. Once the amplitude coefficients are solved for every k_r, the Green's tensor for any configuration of compressional or shear (ring) source potentials can be obtained.

To evaluate the wavenumber integral given by Eq. (14), the complex contour integration technique is applied. The solution can be expressed as a summation of finite number of (normal) modes supplemented by Ewing-Jardetsky-Press (EJP) branch line integrations (Fig. 2(b)). The characteristic equation $f(k_r)$, being the determinant of the coefficient matrix, is used to determine the horizontal wavenumbers $k^{(m)}_r$ (defining the residues' contribution enclosed by the chosen integration path). The final expression of the Green's tensor assuming a unit strength source amplitude reads:

$$\begin{aligned}\tilde{G}(r, z; r_0, z_0, \omega) = -\pi\mathrm{i} \sum_{m=1}^{\infty} \frac{\hat{G}^{\star,num}(k^{(m)}_r, z; z_0)}{f'(k^{(m)}_r)} J_0(k^{(m)}_r\, r_0) H^{(2)}_0(k^{(m)}_r\, r) k^{(m)}_r \\ + \frac{1}{2}\int_{\alpha+\beta} \hat{G}(k_r, z; r_0, z_0) J_0(k_r\, r_0) H^{(2)}_0(k_r\, r) k_r dk_r\end{aligned} \tag{15}$$

in which $\hat{G}^{\star,num}$ denote the numerator of the terms in parentheses of the Green's function in the Hankel domain, $f'(k^{(m)}_r)$ denotes the derivative of the characteristic equation. Finally, the Green's tensor

$\tilde{\mathbf{G}}(r, z; r_0, z_0, \omega)$ can be composed from the individual elements by changing subsequently the position of the source and the receiver points in the layered medium.

3.3 Coupling approach

The Boundary Element Method (BEM) is employed to propagate the given field (obtained from section 3.1) at larger distances. The fundamental solution pair, the Green's displacement and traction tensors $\{\widetilde{U}^{\Xi\xi}_{\alpha\beta}(\boldsymbol{r}, \boldsymbol{r}_0, \omega), \widetilde{T}^{\Xi\xi}_{\alpha\beta}(\boldsymbol{r}, \boldsymbol{r}_0, \omega)\}$, are obatined from the potential functions given the receiver point at $\boldsymbol{r} = (r, z)$ (in medium $\Xi = f$ or s) in α-direction due to a unit impulse at source $\boldsymbol{r}_0 = (r_0, z_0)$ (in medium $\Xi = f$ or s) in β-direction (which yields the coefficients $S^{\xi}_{\beta}(\omega)$ as given in Eq. (12-14)).

The complete solution for the acousto-elastic domain reads ($\alpha = z$ or r):

$$\begin{aligned}\tilde{u}^{\Xi}_{\alpha}(\boldsymbol{r}) = \sum_{\beta=r,z} \int_{S^s} \left(\widetilde{U}^{\Xi s}_{\alpha\beta}(\boldsymbol{r}, \boldsymbol{r}_0, \omega) \cdot \tilde{t}^{\boldsymbol{n}}_{\beta}(\boldsymbol{r}_0, \omega) - \widetilde{T}^{\boldsymbol{n}, \Xi s}_{\alpha\beta}(\boldsymbol{r}, \boldsymbol{r}_0, \omega) \cdot \tilde{u}_{\beta}(\boldsymbol{r}_0, \omega) \right) dS^s_0(\boldsymbol{r}_0) \\ + \int_{S^f} \left(\widetilde{U}^{\Xi f}_{\alpha r}(\boldsymbol{r}, \boldsymbol{r}_0, \omega) \cdot \tilde{p}(\boldsymbol{r}_0, \omega) - \widetilde{T}^{\boldsymbol{n}, \Xi f}_{\alpha r}(\boldsymbol{r}, \boldsymbol{r}_0, \omega) \cdot \tilde{u}_r(\boldsymbol{r}_0, \omega) \right) dS^f_0(\boldsymbol{r}_0),\end{aligned} \tag{16}$$

in which $\tilde{u}$, $\tilde{t}^{\boldsymbol{n}}$ and $\tilde{p}$ are known from the near-source module since all physical quantities have been computed at the surface of the pile.

4. Influence of the seabed conditions on the sound levels

In this section, two cases are examined which are based on a typical configuration for the installation of foundation piles in offshore wind farms. The material properties and the geometry of the model are summarised in Table 1. The input forcing function is given in Fig. 3(b). The seabed for case 1 consists of a thin marine sediment layer overlaying a relatively stiffer bottom soil half-space compared to that of case 2.

Table 1: Input parameters for the case study. Note: the first and second terms in the parentheses show the values of the correspondent parameter for the upper and lower soil layer, respectively.

Parameter	Pile	Parameter	Fluid	Soil (Case 1)	Soil (Case 2)
Length [m]	76	Depth [m]	40	$(4.3, \infty)$	$(0.7, \infty)$
Density [kg m^{-3}]	7850	Density [kg m^{-3}]	1000	$(1680, 1950)$	$(1700, 1900)$
Outer diameter [m]	8	c_p [ms^{-1}]	1500	$(1537, 1977)$	$(1570, 1843)$
Wall thickness [mm]	90	c_s [ms^{-1}]	–	$(95, 369)$	$(99, 282)$
Penetration depth [m]	32	α_p [dBλ^{-1}]	–	$(0.55, 0.27)$	$(0.55, 0.27)$
Hammer blow energy [kJ]	2000	α_s [dBλ^{-1}]	–	$(1.36, 1.09)$	$(1.36, 1.09)$

First, the peak pressure level (L_{peak}) and the sound exposure level (SEL) of receiver points at radial distances up to 750m are shown in Fig. 3(a). The SEL and L_{peak} for case 1 are higher compared to case 2. In Fig. 3(b), the evolution of the pressure field in time is shown for the point positioned 2m above the seabed at 750m from the pile. As can be seen, the arrival of the pressure cones is at around 0.5 sec after the impact of the pile, which is in line with the expectations regarding the arrival time of the direct sound waves travelling with the speed of sound in the water. For the characterization of acoustic energy radiated into the fluid and the seabed, the energy fluxes through cylindrical surfaces positioned at two radial distances are shown in Fig. 4. At close ranges, the energy flux along the depth grows steeply at the

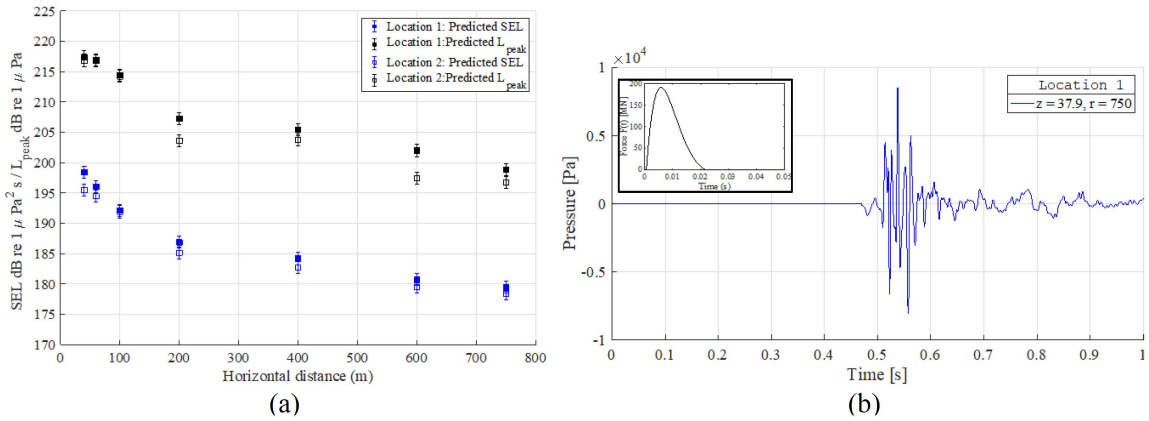

Figure 3: (a) Comparison of SEL and L_{peak} at several radial distances from the pile and 2 m above the seabed for cases 1 and 2; and (b) evolution of the pressure field at 750m from the pile (case 1).

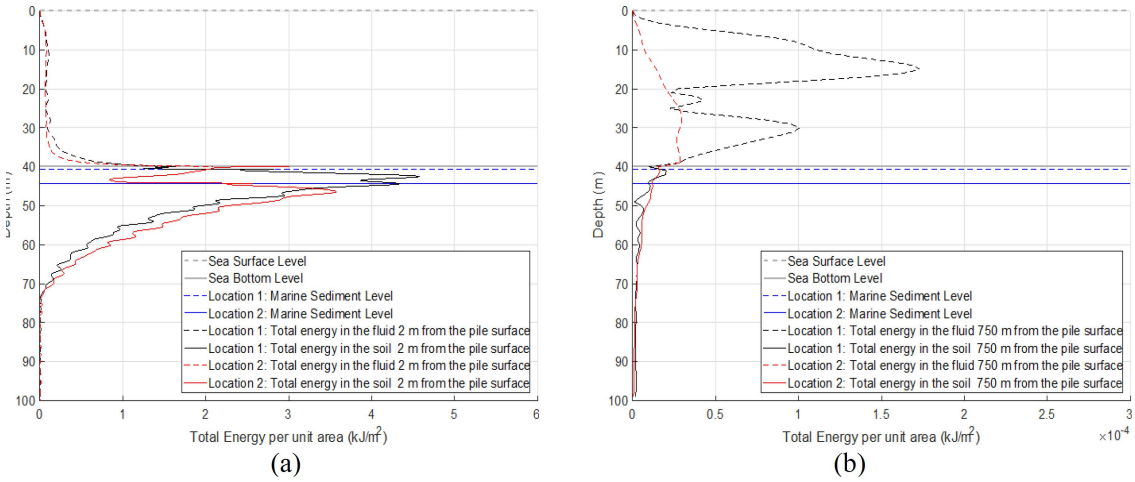

Figure 4: Energy flux through a cylindrical surface positioned at (a) 2m from the pile surface; and (b) 750m from the pile surface.

level of transition from fluid to soil. As shown in Fig. 4(a), there is considerable energy concentration close to the seabed-water interface at the vicinity of the pile caused by the presence of the Scholte waves which dominate the response at the interface. However, an examination of the flux at a larger distance (Fig. 4(b)) shows that the contribution of acoustic energy from interface waves diminishes with distance. As waves propagate away from the pile, the energy flux in the water is proportionally larger than the one through the soil due to the higher energy losses in the latter medium. This physical interpretation emphasizes the significance of the position of the noise mitigation system; the further it is positioned from the pile, the more effective it is expected to be. Next to that we note that in the close range, the stiffer the soil, the higher amount of energy that is radiated directly in the water column.

5. Conclusions

The paper examines the influence of the soil conditions on the near- and far-field sound propagation generated by impact piling. A computationally efficient approach is presented for noise predictions by

offshore pile driving. The mathematical statement of the complete problem is given and the adopted method of solution is described. Results are presented for a typical installation scenario with varying soil conditions. An energy flux analysis shows the energy radiation into the seabed and seawater as well as the evolution of this energy balance at larger (from the pile) distances. This evaluation is important for accessing the sound transmission paths which is key for the effective mitigation of the noise. The results indicate that the stiffer the seabed, the higher the sound pressure levels in the seawater. In the future, model predictions will be benchmarked against available data from measurement campaigns published in the scientific literature.

6. Acknowledgements

The authors gratefully acknowledge China Scholarship Council (CSC) for financing this research project on the development of a generic underwater noise prediction model for offshore activities.

REFERENCES

1. Bailey, H., Senior, B., Simmons, D., Rusin, J., Picken, G. and Thompson, P. M. Assessing underwater noise levels during pile-driving at an offshore windfarm and its potential effects on marine mammals, *Marine Pollution Bulletin*, (2010).

2. Lippert, S., et al. COMPILE—A Generic Benchmark Case for Predictions of Marine Pile-Driving Noise, *IEEE Journal of Oceanic Engineering*, **41** (4), 1061–1071, (2016).

3. Reinhall, P. G. and Dahl, P. H. Underwater Mach wave radiation from impact pile driving: Theory and observation, *The Journal of the Acoustical Society of America*, **130** (3), 1209–1216, (2011).

4. Tsouvalas, A. and Metrikine, A. V. A three-dimensional vibroacoustic model for the prediction of underwater noise from offshore pile driving, *Journal of Sound and Vibration*, **333** (8), 2283–2311, (2014).

5. Peng, Y., Tsouvalas, A., Stampoultzoglou, T. and Metrikine, A. Study of the sound escape with the use of an air bubble curtain in offshore pile driving, *Journal of Marine Science and Engineering*, **9** (2), (2021).

6. Peng, Y., Tsouvalas, A., Stampoultzoglou, T. and Metrikine, A. A fast computational model for near- and far-field noise prediction due to offshore pile driving, *The Journal of the Acoustical Society of America*, **149** (3), 1772–1790, (2021).

7. Tsouvalas, A. and Metrikine, A. Structure-Borne Wave Radiation by Impact and Vibratory Piling in Offshore Installations: From Sound Prediction to Auditory Damage, *Journal of Marine Science and Engineering*, **4** (3), 44, (2016).

8. Tsouvalas, A., van Dalen, K. N. and Metrikine, A. V. The significance of the evanescent spectrum in structure-waveguide interaction problems, *The Journal of the Acoustical Society of America*, (2015).

9. Nealy, J. L., Collis, J. M. and Frank, S. D. Normal mode solutions for seismo-acoustic propagation resulting from shear and combined wave point sources, *The Journal of the Acoustical Society of America*, (2016).